Parameterized model to approximate theoretical collision-induced absorption band shapes for O2-O2 and O2-N2

Erin Adkins, Tijs Karman, Alain Campargue, Didier Mondelain, Joseph Hodges

Parameterized Model to Approximate Theoretical Collision-Induced Absorption Band Shapes for O_2-O_2 and O_2-N_2

Erin M. Adkins[1], Tijs Karman[2], Alain Campargue[3], Didier Mondelain[3], and Joseph T. Hodges[1]

[1]Chemical Sciences Division, National Institute of Standards and Technology, Gaithersburg, Maryland 20899 U.S.A.

[2]Institute for Molecules and Materials, Radboud University, Nijmegen, the Netherlands

[3]Univ. Grenoble Alpes, CNRS, LIPhy, 38000 Grenoble, France

5/23/23

Abstract

Collision-induced absorption from vibronic transitions of O_2-O_2 and O_2-N_2 collision complexes is an important contributor to light-matter interaction in the atmosphere with relevance to radiative heat transfer and spectroscopic remote sensing. Despite in-depth studies involving quantum calculations of this effect, comparisons between experiment and theory would benefit from less computationally burdensome calculations that closely approximate the temperature dependence of the theoretical band shape and intensity. Accordingly, we present a parameterized representation of recent quantum calculations for collision-induced absorption by O_2-O_2 and O_2-N_2 about the 1.27 μm monomer band of O_2. This approach leverages the theoretical decomposition of the spectra into exchange and spin-orbit contributions, with each component having a distinct temperature-dependent band shape. Composite spectra are approximated as a linear combination of the theoretical profiles with seven adjustable parameters that scale the component intensities and their dependences on temperature. We demonstrate that this empirical representation can accurately simulate the theoretical calculations, and we present a global fit of the model to previously reported collision-induced absorption spectra (O_2-O_2, O_2-N_2, and O_2-air) measured by cavity ring-down spectroscopy over the temperature range 271 K - 332 K.

Introduction

By exploiting the well-mixed quality of molecular oxygen in the atmosphere, spectroscopic measurements of light absorption can provide a precise measure of column-integrated air mass for satellite and remote sensing missions. To this end, the rovibronic O_2 A-band, $b^1\,\Sigma^-_g$ -$X^3\Sigma^-_g$ (0 – 0), centered at a wavelength of 0.76 μm, is used by the OCO-2 [1], OCO-3 [2], GOSAT [3], and SCIAMACHY [4] missions. Similarly, the rovibronic 1.27 μm band of O_2, $a^1\Delta_g$-$X^3\Sigma^-_g$ (0 – 0), has been probed to determine air mass in the ground-based Total Carbon Column Observing Network (TCCON) [5], whereas recent advances in modeling spontaneous emission from excited state O_2 in the upper atmosphere (airglow) [6, 7] have enabled use of this band in satellite measurements such as the COCCON [8], SCIAMACHY [4], and MicroCarb missions [9].

Atmospheric column retrievals rely on the ability to accurately model variations of the O_2 absorption coefficient with frequency, pressure, temperature, and collisional partner, as well as to account for complications associated with line mixing and underlying continua. Observed spectra exhibit narrow monomer lines characteristic of each rovibronic band which are superimposed on a broad collision-induced absorption (CIA) continuum. The monomer rovibronic transitions in both bands are caused by weak spin-orbit-allowed magnetic dipole transitions [10]. In the atmosphere, the CIA continuum in these bands is caused by binary collisions between O_2-O_2 or O_2-N_2 molecules resulting in a transient collisional

complex with an electric dipole transition moment. While the absorption coefficient of each monomer line is proportional to O_2 molecular density, that of the CIA is proportional to the product of the number densities of O_2 and its collisional partner either O_2 or N_2 in this case. This property makes the phenomena increasingly important at high density, like those found in remote sensing measurements [11].

Traditionally, CIA in these O_2 bands is operationally defined as the absorption that remains after accounting for baseline, monomer absorption, and other losses like Rayleigh scattering [10, 12-17] in observed spectra. This approach can present difficulties in systems like the O_2 A-band, where the CIA is relatively weak by comparison to the monomer contribution and its extraction from the measured spectrum is highly correlated with the chosen line-mixing model [18-20]. Consequently, retrievals of CIA depend on spectroscopic relations that describe the *J*-dependence of the intensities, line shapes and line mixing of the monomeric spectra. The inclusion of theoretical constraints on the magnitude and shape of the CIA is expected to help decouple the concurrently observed monomeric and bimolecular features, which should ultimately lead to more accurate measurements of the CIA and improved spectroscopic models.

While models of spectroscopic lines shapes have long been used to describe monomer transitions [21], until recently published work by Karman *et al*. [10], a well-developed theory did not exist for modeling the band shape of spin-forbidden electronic transitions in bimolecular collisions. To address this gap, they used analytical models and numerical quantum scattering calculations to calculate the band shape of CIA for O_2-O_2 and O_2-N_2 collision pairs in both the 0.76 μm (0 – 0) and 1.27 μm O_2 bands (0–0), as well as in the three vibrationally excited upper state bands: [(0–1), (0–2) for $a^1\Delta_g$-$X^3\Sigma^-_g$] and [(0–1) for $b^1\,\Sigma^-_g$ -$X^3\Sigma^-_g$] [10]. This theoretical model is based on the superposition of two distinct interaction mechanisms: exchange and spin-orbit [10]. The exchange mechanism accounts for the exchange interaction between paramagnetic collisional partners and yields a much broader band shape than the spin-orbit case which corresponds to intramolecular spin-orbit coupling between various states of O_2 [10]. Because the exchange mechanism only applies to paramagnetic collisional partners, the CIA by O_2-O_2 is predicted to have both spin-orbit and exchange components, but that of O_2-N_2 will only have a spin-orbit component [10]. The accuracy of the predicted band shapes for both mechanisms is limited by the approximations in the modeling, while the intensities of the mechanisms are subject to relatively large uncertainty in the dipole moment surfaces. Because of these uncertainties, the intensities of the spin-orbit and exchange mechanisms are scaled and summed to best match measured spectra [10, 11, 14, 18, 22, 23].

By comparison to the 0.76 μm O_2 band, absorption in the 1.27 μm band exhibits a much more prominent CIA continuum relative to its monomer spectrum, with the latter component exhibiting less line-mixing. These properties of the 1.27 μm band facilitate disentanglement of the monomeric and its CIA contributions to total absorption – thus rendering this band to be a more appropriate initial case for assessing the accuracy of theoretical calculations of CIA involving O_2. In the remainder of this article, we focus on CIA in the 1.27 μm band, and we apply the theoretical calculations of Karman *et al* [10] to analyze three sets of previously published cavity ring-down spectroscopy (CRDS) measurements which comprise CIA spectra in O_2-O_2, O_2-N_2 and O_2-air samples for temperatures ranging from 271 K – 332 K. To illustrate this approach, we present a multiparameter and intensity-scalable approximation yielding results that accurately simulate those given by theory, we use this model approximation to globally fit rescaled CIA band shapes to the measured spectra, and we discuss how the presented model can support intercomparisons between new experiments and theory.

Experimental and Theoretical CIA

Here we compare the theoretical spectra published in [10, 11] to four sets of measured CIA in the 1.27 μm O_2 band corresponding respectively to Maté *et al*. [14], Mondelain *et al*. [13], Kassi *et al* [12], and Fleurbaey *et al* [24]. The experiments of Maté *et al*. were done using Fourier transform spectroscopy (FTS) [14], and the other three cited studies were based on CRDS [12, 13, 24].

Maté *et al*. measured O_2-O_2 and O_2-N_2 CIA at sample densities between 1 and 10 amagat, and temperatures, *T*, of 253 K, 273 K, and 296 K [14]. A density in amagat units is defined as the ratio of the observed ideal-gas number density at a temperature, *T*, and pressure, *p*, with that at a reference condition of 273.15 K and 101.325 kPa. The monomer absorption of O_2 was modeled using the spectroscopic line list of Lafferty *et al*. [25] with adjustments to the Q-branch line intensities introduced to minimize residuals and N_2-broadening parameters approximated from the self-broadening [14]. The CIA spectra for O_2-O_2 at 296 K and O_2-air at 253 K, 273 K, and 296 K published by Maté are included in HITRAN 2019 CIA update [11].

Regarding the theoretical CIA calculations of Karman *et al.*, because there are significant uncertainties in the calculated dipole moment surfaces, the intensities of the spin-orbit and exchange components are also subject to large uncertainty. Consequently, the 1.27 μm band CIA intensities [10] were scaled to the measurements reported by Maté *et al*. [14], and these results were published in the HITRAN 2019 CIA update over the temperature range 206 K – 346 K for the O_2-O_2, O_2-N_2, and O_2-air systems [11]. In the remainder of this article, references to the "theoretical" CIA for this band correspond to these intensity-scaled results. The spin-orbit and exchange band shapes across the same temperature range are provided in the supplement of this work.

In the initial CRDS study of CIA in the 1.27 μm O_2 band, Mondelain *et al*. reported O_2-N_2 and O_2-O_2 measurements collected at 297 K [13], while in a second study by the same group Kassi *et al*. provided additional measurements at 271 K and 332 K [12]. The broad wavenumber ranges covered, 7,550 cm^{-1} – 8,360 cm^{-1} at 271 K and 332 K, and 7513 cm^{-1} – 8466 cm^{-1} at 297 K, were achieved using a combination of distributed feedback and external cavity diode lasers. Unlike the Maté *et al*. data [14], these spectra were collected below 1 amagat (which is more representative of atmospheric conditions), and measurements were made in the troughs between the monomer absorption lines. As described above, the CIA was determined as the remaining absorption after having subtracted the measured Rayleigh scattering and monomer absorption [26, 27]. The reported binary collision absorption coefficient was based on a spline fit to the CIA measurements in the trough segments.

The most recent study of CIA in the 1.27 μm O_2 band by Fleurbaey *et al*. [24] was based on frequency-stabilized CRDS. Measurements of O_2 in air at 296 K were made at six pressures from 3.3 kPa to 100 kPa and covering the spectral range 7800 cm^{-1} – 7950 cm^{-1}. Unlike the previous measurements by Mondelain *et al*. [13] and Kassi *et al*. [12], the monomer absorption cores and regions between transitions were measured. In this study, the line shape parameters of the monomer transitions were fit and the CIA was extracted from smoothed baseline fits over small wavenumber segments (1 cm^{-1} – 2 cm^{-1}) [24].

Comparison between the Theoretical CIA and Experimental Datasets

In the left column of Fig. 1 we present the theoretical CIA data, where it is apparent that the integrated O_2-O_2 CIA is about four times larger than the O_2-N_2 component, with O_2-air component being about three times smaller than that of the air after summing the O_2 and N_2 contributions weighted by their respective mole fractions. On the scale of the relatively large differences in integrated CIA between the O_2-broadener pairs, the impact of temperature is much smaller, but not entirely negligible.

In the right column of Fig. 1 we summarize the differences (observed – theory) in binary absorption coefficients between the four above-mentioned experimental studies and the theoretical values for O_2-O_2, O_2-air, and O_2-N_2 using the previously scaled mechanism intensities. For all broadener pairing it is evident that the CRDS results exhibit significantly less noise than do the data of Maté *et al*, which can be attributed in part to the fact the CRDS results have been smoothed. There is excellent agreement between the room-temperature O_2-air binary absorption coefficients reported by Mondelain *et al*. [13] and those of Fleurbaey *et al*. [24], where the integrated binary absorption coefficients have a relative absolute difference of 0.11% over the common spectral range [24]. The O_2-air binary absorption coefficient reported by Maté *et al*. [14] is about 3% smaller than that reported at similar temperatures by Mondelain [13] and Kassi [12]. Near a temperature of 296 K, the O_2-O_2 binary absorption coefficient is about 2.5% smaller than that reported by Mondelain [13] and 0.5% smaller than that reported by Kassi [12] close to 273 K.

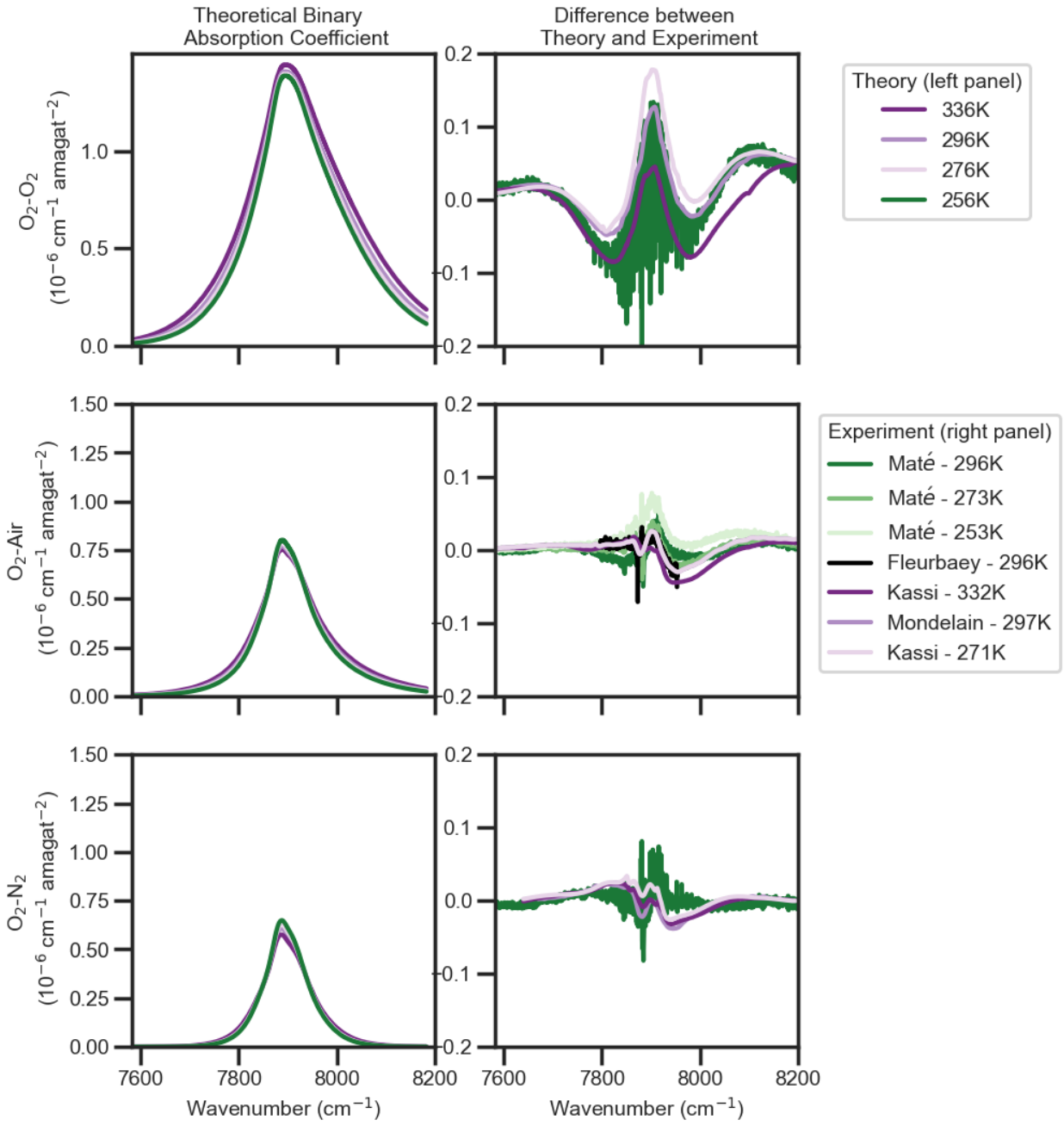

144

145 **Fig. 1**. Theoretical CIA binary absorption coefficients [10, 11] (left panels) at range of temperature similar to
146 experimental data. Differences between experimental and theoretical (obs. – calc.) CIA binary absorption
147 coefficients for Maté [14], Mondelain [13], Kassi [12], and Fleurbaey [24] data (right panels). The band center is
148 located at approximately 7875 cm^{-1}.

149 There is good agreement between the theoretical values and the experimental datasets with relative
150 magnitude of the residuals at approximately the 5-12 % level, shown in Fig. 1. This comparison has zero
151 degrees of freedom, which makes this level of agreement promising for use of theoretical values in the
152 analysis of experimental CIA spectra. Despite the agreement, there are systematic differences between
153 the experiment and theory. The O_2-O_2 binary absorption coefficient shows the largest difference with
154 structured symmetric *w*-shaped residuals. For the case of O_2-air, these differences exhibit an asymmetric

w shape with the larger lobe on the R-branch side. The lower-magnitude and narrower lobe observed is located at the Q Branch, located approximately between 7865 cm^{-1} and 7885 cm^{-1}, where there is a high density of lines. This is a spectral region where the discrepancy between the theory and measurements could be especially susceptible to choice of the monomer absorption model, specifically line mixing [10]. The O_2-N_2 binary absorption coefficient residual also exhibits a large asymmetric *w*-shaped difference. Notably, the data are of sufficiently high quality that all collision-partner pairings show a temperature dependence in the residuals.

Based on the systematic differences between experiment and the published theory shown in Fig. 1 (which vary with temperature), it is apparent that additional degrees of freedom in the model are needed to improve the agreement between observations and calculations. In the approach used by Karman *et al.* [10], only the spin-orbit and exchange mechanism intensities were scaled to match the observations, and no provisions for adjusting the temperature dependence of these intensities were considered. To address this limitation, below we introduce an adjustable model to specify small deviations of the temperature dependence about the theoretical behavior.

Defining the Model Function

We define the binary absorption coefficient, *B*, for each collision pair (either O_2-O_2 or O_2-N_2) and CIA mechanism (spin or exchange) as the ratio of the absorption coefficient, α, and the product of absorber and collision-partner number densities, ρ_{O2}^2 or $\rho_{O2}\rho_{N2}$. Using the theoretical CIA model for the 1.27 μm O_2 band reported by Karman *et al*. [10] we account for the temperature (T) and wavenumber (ν) -dependent spin-orbit and exchange mechanisms described by the theoretical area-normalized profiles $g_s(\nu,T)$ and $g_e(\nu,T)$, (in cm) respectively, with the relative intensities for the spin-orbit, S_s and exchange S_e components scaled to match the measurements (in cm^{-2} $amagat^{-2}$). This decomposition leads to binary absorption coefficients (in units of cm^{-1} $amagat^{-2}$) for O_2-O_2 (Eq. 1) and O_2-N_2 (Eq. 2). It should be noted that the spin-orbit area-normalized profile is the same for both O_2-O_2 and O_2-N_2, but the intensity of the spin-orbit component is unique to the collisional pair.

$$\alpha_{O2-O2}/\rho_{O2}^2 = B_{O2-O2} = S_{O2-O2,s}\, g_s + S_{O2-O2,e}\, g_e \quad (1)$$

$$\alpha_{O2-N2}/(\rho_{O2}\rho_{N2}) = B_{O2-N2} = S_{O2-N2,s}\, g_s \quad (2)$$

The binary absorption coefficient of an arbitrary mixture of O_2 and N_2, designated by *x*, is given by the mole-fraction-weighted sum of O_2-O_2 and O_2-N_2 binary absorption coefficients in Eqs. 1-2

$$B_{O2-x} = \chi_{O2}(S_{O2-O2,s}\, g_s + S_{O2-O2,e}\, g_e) + \chi_{N2}\, S_{O2-N2,s}\, g_s \quad (3)$$

$$= \chi_{O2}\, B_{O2-O2} + (1-\chi_{O2})B_{O2-N2},$$

where $\chi_{O2} = \rho_{O2}/\rho_{tot}$, $\chi_{N2} = \rho_{N2}/\rho_{tot} = 1-\chi_{O2}$ are the respective mole fractions of O_2 and N_2 in the mixture and $S_{O2-O2,s}$, $S_{O2-O2,e}$, and $S_{O2-N2,s}$ comprise the set of three mechanism-dependent intensities. Note that, with the aid of Eqs. 1 and 3, independent measurements of B_{O2-O2} and B_{O2-x} can be used to extract experimental values for B_{O2-N2} and B_{O2-Air}. In this work we treat air as a binary mixture of O_2 (mole fraction of 0.2095) and N_2, ignoring the effects of Ar and other species.

Generally, the magnitude of the CIA is reported in terms of the integrated binary absorption coefficient, $\int B_{O2-m}(\nu;T)d\,\nu$. If the g_s and g_e profiles are area-normalized in the model function, then the integrated binary absorption coefficient must equal the sum of the intensities from the spin-orbit and ex-

change mechanisms. The temperature dependence of the spin-orbit and exchange band shape functions over the temperature range 206 K – 346 K, are extrapolated to a broader spectral range to provide a more accurate measure of the mechanism area [10, 11]. These results are given in the supplemental material. Each extrapolated spin-orbit and exchange mechanism at a given temperature was normalized by area so that $\int g(\nu;T)d\,\nu = 1$.

The spectrum profiles for the exchange and spin-orbit mechanisms depend on temperature and are provided in the supplement in 10 K increments between 206 K and 346 K. Without a functional form that captures changes in band shape with temperature, an interpolation function is necessary to estimate the theoretical shape of g_s and g_e at an arbitrary temperature within the temperature range considered in the theory. For both mechanism band shapes and at each sampled wavenumber, we fit a third-order polynomial, Eq. 4, to the ratio of area-normalized profile at a temperature with that at the reference temperature, T_r = 296 K. The fitted coefficients were tabulated for use in the parameterized CIA model. Fig. 2 shows the relative change in the area-normalized band shapes as a function of temperature at several discrete wavenumbers across the spectral region considered.

$$g_m(\nu;T) = g_{m,r}(\nu)\,[1 + b_m(\nu)\cdot(T-T_r) + c_m(\nu)\cdot(T-T_r)^2 + d_m(\nu)\cdot(T-T_r)^3], \quad (4)$$

where, $\int g_m(\nu;T)d\,\nu = 1$, in which m designates exchange or spin-orbit, and r refers to the reference temperature condition T_r = 296 K.

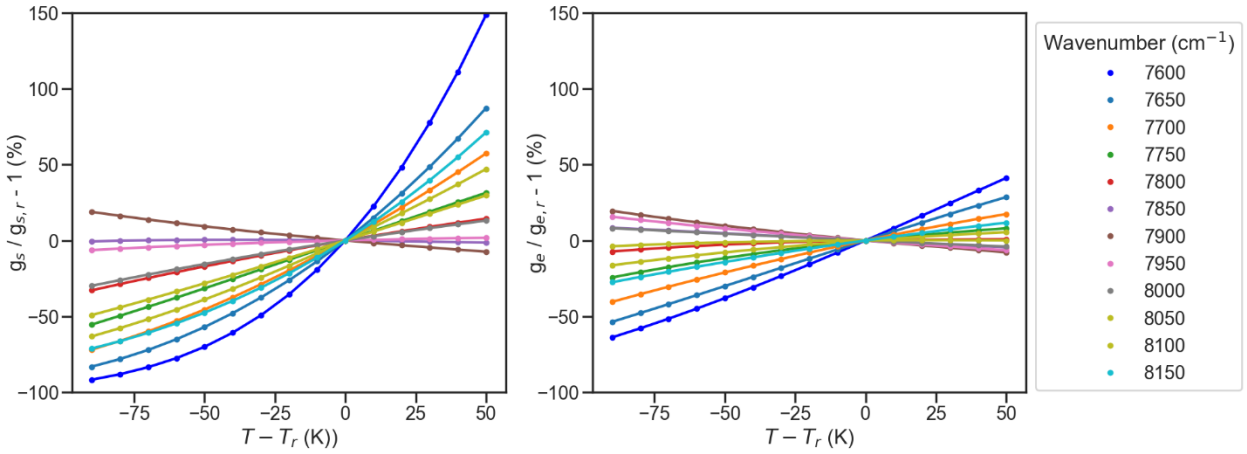

Fig. 2. Least-squares fits of Eq. 4 to the temperature-dependent theoretical spin-orbit (left) and exchange (right) mechanism band shapes assuming a reference temperature of 296 K. Calculations are shown for various wavenumbers across the 1.27 μm O_2 band. Fitted and theoretical results are indicated by solid lines and symbols, respectively.

In addition to capturing the temperature dependence of the two mechanism band shapes, our model treats the three intensities, $S_{O2\text{-}O2,e}$, $S_{O2\text{-}O2,s}$, and $S_{O2\text{-}N2,s}$, as independently adjustable, temperature-dependent parameters. To demonstrate that this approach provides an accurate representation of the theoretical spectra as a function of wavenumber and temperature, we fit the sum of g_s and g_e terms scaled by the respective three intensities to the binary absorption coefficients published by Karman *et al.* [10, 11]. The resulting fit residuals were at the numerical noise level, as the theoretical binary absorption coefficients were similarly generated. The temperature dependence for each of the three intensities was subsequently described as a second-order polynomial relative to the value at the reference temperature, given by expressions of the form

$$S_m(T) = S_m(T_r)[1 + e_m \cdot (T - T_r) + f_m \cdot (T - T_r)^2]. \quad (5)$$

The adjustable terms derived from this fitting procedure are summarized in Table 1, and the temperature dependences of the intensities for both the spin-orbit and exchange mechanisms are plotted in Fig. 3. We note that when normalized to the reference temperature, the spin-orbit mechanism intensity is assumed to have the same temperature dependence for O_2-O_2 and O_2-N_2, despite differences in their respective intensities. This constraint could be relaxed if sufficient data spanning a range of sample compositions and experimental temperatures were available for validation.

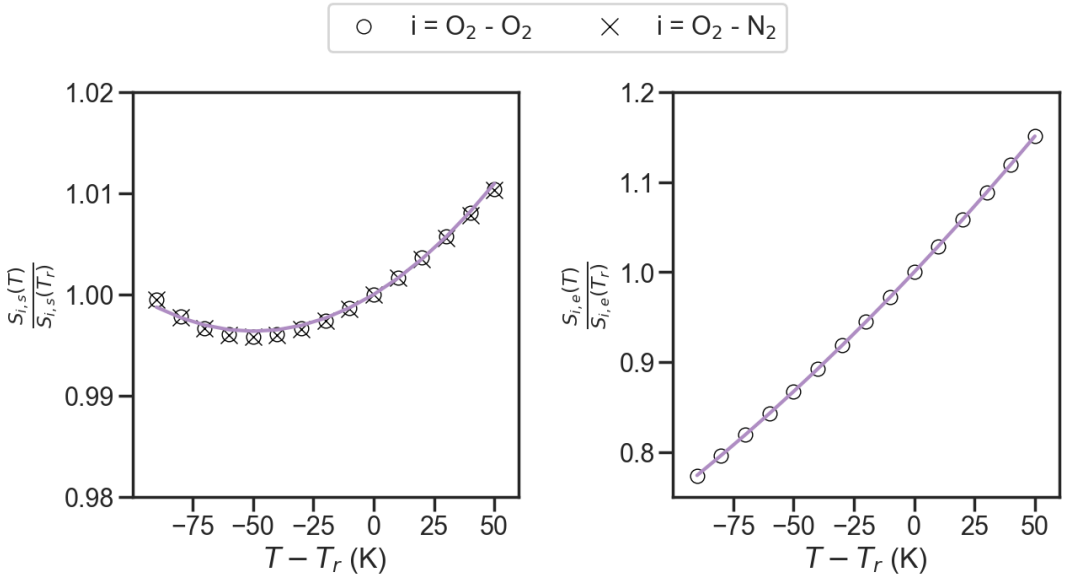

Fig. 3. Least-squares fits of Eq. 5 (solid lines) to the theoretical normalized temperature-dependent integrated intensities (symbols) for the spin-orbit (left) and exchange mechanisms (right). The theorical spin-orbit normalized temperature-dependent integrated intensity is the same for O_2-O_2 and O_2-N_2, resulting in overlayed symbols.

The combination of area-normalized band shapes, $g_s(\nu,T)$ and $g_e(\nu,T)$, plus the ability to calculate their respective temperature-dependent intensities, provides sufficient flexibility to numerically represent the composition, temperature and wavenumber dependences of the theoretical CIA reported by Karman *et al*. [10]. To this end, we can use Eq. 4 to calculate the normalized g_s and g_e at the experimental temperature which enables the composite profiles to be interpolated onto the experimental wavenumber grid. The intensity terms, $S_{O2\text{-}O2,e}$, $S_{O2\text{-}O2,s}$, and $S_{O2\text{-}N2,s}$, and associated sets of intensity temperature dependence parameters e_s, $f_{s,}$, e_e, and f_e, for each absorber-collision pair can then be adjusted to yield a best-fit to the experimental binary coefficients.

Fitting the Model to the Combined Grenoble and NIST data

To assess whether our parameterized models can provide a precise representation of experimental results, we fit this model to the combined results of Fleurbaey *et al.* [28], Mondelain *et al.* [13], and Kassi *et al.* [12]. The data of Mondelain (at 297 K) [13] and Kassi (at 271 K and 332 K) [12] were obtained for samples of O_2-N_2 and O_2-O_2. The Q-branch region of these data was omitted based on the required interpolation in this congested spectral interval. While the Fleurbaey [24] data are only available at 296 K and for O_2-air, they provided information in the Q-branch window because of the full-band collection procedure.

In an initial analysis, the intensity terms were adjusted to best match the measurements, but their temperature-dependence parameters were constrained to the theoretical values described above. The results are shown in Fig. 4(b). Allowing the intensities to vary to match the experimental spectra decreases the magnitude of the residuals for broadener pairs compared to the evaluation with the theoretical values. However, band-wide systematic residuals remain. Additionally, the magnitude of the residuals shows a temperature dependence, most notably for the case of O_2-O_2.

As illustrated in Fig. 4c, adjustment of the reference intensity and intensity temperature dependence terms reduces the temperature dependence of the fit residuals although systematic broadband residuals remain. The O_2-O_2 binary absorption coefficient has a symmetric *w*-shaped residual, whereas that for O_2-air has an asymmetric *w*-shaped residual with a larger broader lobe on the R-branch side. Notably, our current parameterization of the theoretical CIA does not allow for the mechanism band shapes to be adjusted. This results in an underestimation of the integrated binary absorption coefficients for O_2-O_2, O_2-air, and O_2-N_2 by 2.7%, 2.1%, and 1.2% when compared to the values reported at the reference temperature by Mondelain et al [13].

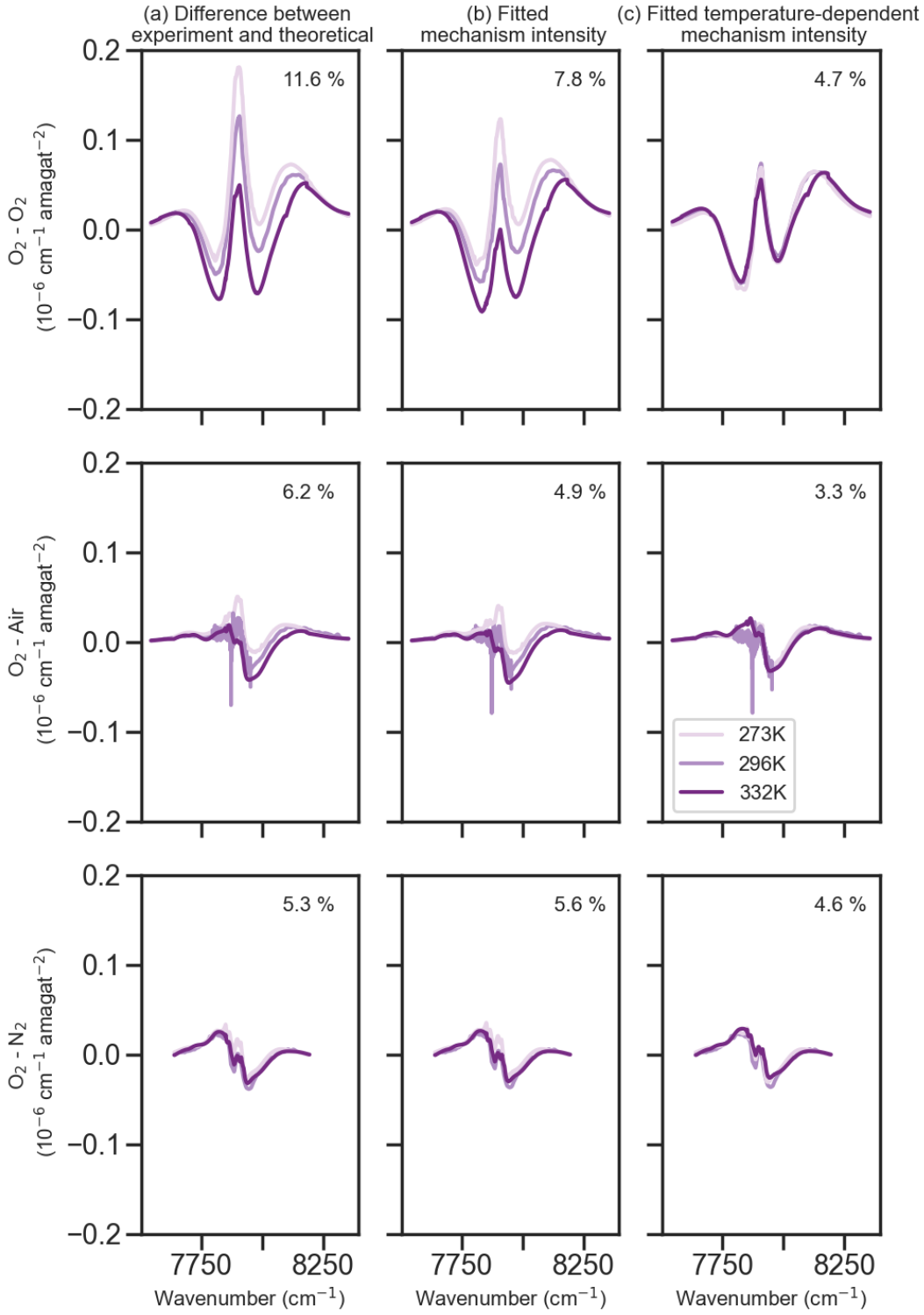

Fig. 4. Least-squares fits of the intensity-scaled, theoretical binary absorption coefficient, B_{O2-x}, with the combined CRDS data from Fleurbaey [24], Mondelain [13], and Kassi [12]. (a) Spin-orbit and exchange temperature-dependent intensities were constrained to theory (left). (b) Spin-orbit and exchange intensities were constrained to follow the theoretical temperature dependence and only the reference intensities were floated (center). (c) Results

obtained by also floating the temperature dependence of the intensities (right). The three panels are the fit residuals for O_2-O_2, O_2-air, and O_2-N_2 (obs. – calc.). The relative magnitude of the residuals (max. – min. / obs.) is presented in top right corner of each subplot.

Table 1. Mechanism intensities and intensity temperature dependence terms based on 1) theory scaled to Maté *et al*. [14]and 2) values obtained from fitting the parameterized model to the Mondelain *et al*.[13], Kassi *et al.*[12], and Fleurbaey *et al.* [24] data sets.

	$S_{O2\text{-}O2,e}$ (10^{-6} cm^{-2} amagat^{-2})	$S_{O2\text{-}O2,s}$ (10^{-6} cm^{-2} amagat^{-2})	$S_{O2\text{-}N2,s}$ (10^{-6} cm^{-2} amagat^{-2})	e_e	f_e	e_s	f_s
Theory	304.7450(13)	39.1291(9)	70.7353(4)	0.002844(1)	3.63(2) x 10^{-6}	1.46(3) x 10^{-4}	1.47(4) x 10^{-6}
Results from global fit	301.06(31)	48.00(19)	70.27(4)	0.00128(3)	6.7(13) x 10^{-6}	-4.5(6)x 10^{-4}	9.1(18) x 10^{-6}

Table 1 compares the theoretical values for the mechanism intensities and intensity temperature dependence parameters to those resulting from global fits to the data [12, 13, 24]. The O_2-air integrated binary absorption coefficients from Mondelain *et al*. [13] and Fleurbaey *et al*. [24] were within 0.11%. Additionally, the data of Mondelain [13] *et al*. were collected at the reference temperature condition, making it an ideal comparison point. The integrated binary absorption coefficients (obtained without adjusting the temperature dependence of the band shape to fit the experimental data) reported for the scaled theoretical model [11] were 4.2%, 2.6%, and 0.5% smaller than the measured values reported by Mondelain *et al*. [13] for the O_2-O_2, O_2-air, and O_2-N_2 cases, respectively. Fits to the same data including adjustment of both the mechanism intensities and their temperature dependences, yielded relative differences between experiment and model of 2.7%, 2.1%, and 1.2%, for the O_2-O_2, O_2-air, and O_2-N_2 pairs, respectively. As before, all three fitted values were smaller than the corresponding measurements reported by Mondelain *et al*. [13]. Given that the fit residuals shown in Fig. 3 for O_2-O_2 are by far the largest among these three collision pairs, not surprisingly we found the biggest improvement was realized for the case of O_2-O_2. The remaining discrepancy in the integrated binary absorption coefficients can be ascribed to the systematic residuals.

Fig. 5 summarizes differences in the temperature dependence of the theoretical and experimental intensities. The results agree with the observations of Kassi *et al*. [12] who suggested that the theoretical temperature dependence of the exchange mechanism was larger than that observed in the experiment and/or the negative magnitude spin-orbit temperature dependence at bandcenter was underestimated. Our analysis (Fig. 5) shows a weaker temperature dependence for the exchange mechanism and a larger-magnitude and opposite slope temperature dependence for the spin-orbit mechanism than that reported by the theory. However, the cavity ring-down CIA data used in this work cover a relatively narrow 60 K interval about the reference temperature and as such do not sample the entire theoretical temperature dependence range. Fig. 2 shows that within this range, temperature-driven changes in the mechanism band shapes are relatively small compared to the broader temperature range where theoretical values were provided. Although there were no physical constraints on the deviation from the theoretical temperature dependence (first- and second-order quadratic terms in Eq. 5), the resulting fitted values were not substantially different than the theoretical values. Consequently, these extra degrees of freedom yielded only small perturbations to the theory. The need for only small changes to the theory to best match experiment highlights the level of agreement between theory and experiment. Our results show that the structure and magnitude of the remaining residuals (after having fit all seven degrees of freedom in the model) appear

to be insensitive to temperature. Expanding the temperature range would improve confidence in the three fitted temperature-dependent intensities and would enable a more rigorous analysis of whether the remaining residual structure is indeed temperature independent.

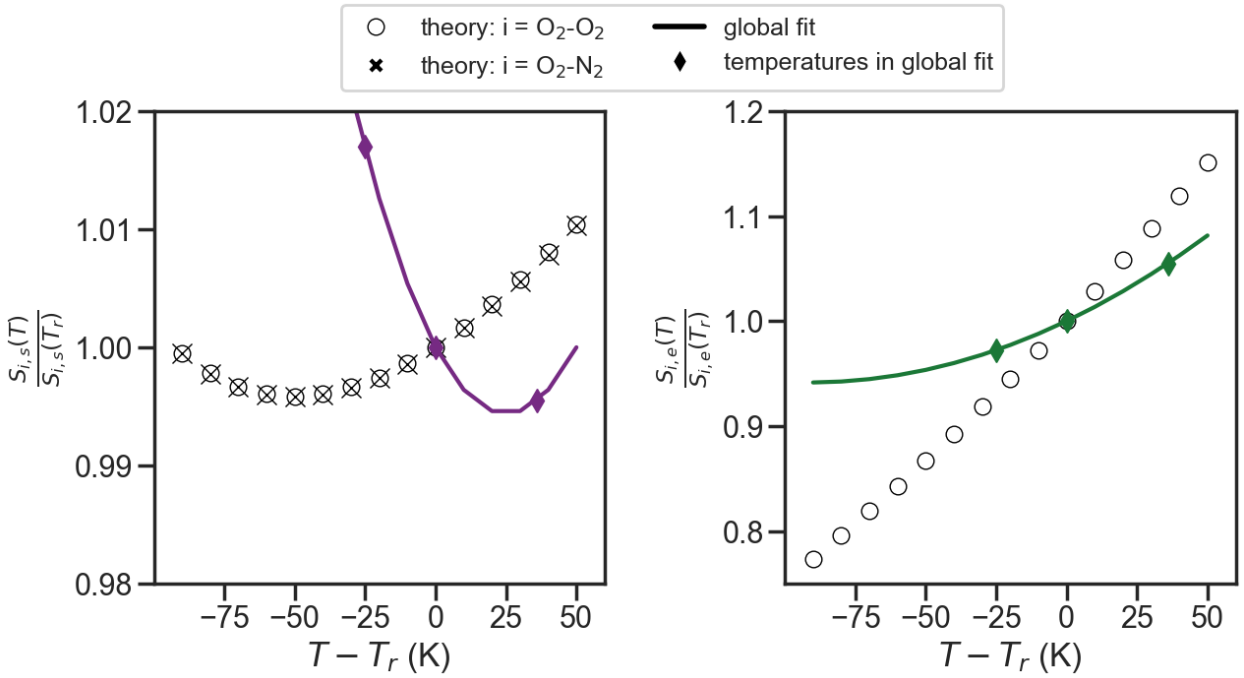

Fig. 5. Comparison of the scalar temperature dependence between theory (based on published temperature dependence, shown with black symbols) and values obtained from global fit (with additional temperature dependence, shown with colored symbols and solid line) to the CRDS data. The theoretical scalar temperature dependence is parameterized by the scalar temperature dependence terms provided in the top row of Table 1. The global fit scalar temperature dependence terms are provided in the bottom row of Table 1.

A current limitation of the parameterized binary absorption coefficient model theory published by Karman *et al*. [10] is the occurrence of systematic structure in the residuals for all broadener pairings. To illustrate this result, Fig. 6 shows the smoothed intensity-normalized residuals of both the spin-orbit and exchange mechanisms. The spin-orbit mechanism residuals were calculated from the O_2-N_2 binary absorption coefficient residuals (Eq 2) based on the global fit to the combined CRDS data [12, 13, 24] . Using this result and the fact that the spin-orbit band shape is independent of collisional pairing, the exchange mechanism residuals were calculated from the O_2-O_2 binary absorption coefficient residuals (Eq 1). While differences between theory and experiment could be addressed by adding empirical adjustments or *ad hoc* corrections to mechanism band shapes, this approach would reduce confidence in using the theoretical band shape as a physical constraint in applications where monomer absorption and CIA are spectrally overlapped and consequently numerically correlated. Accepting that there are limits to the accuracy of theoretical CIA band shapes, then the structure and magnitude of the fit residuals can provide insight into refining the theory and quantifying any resulting improvements.

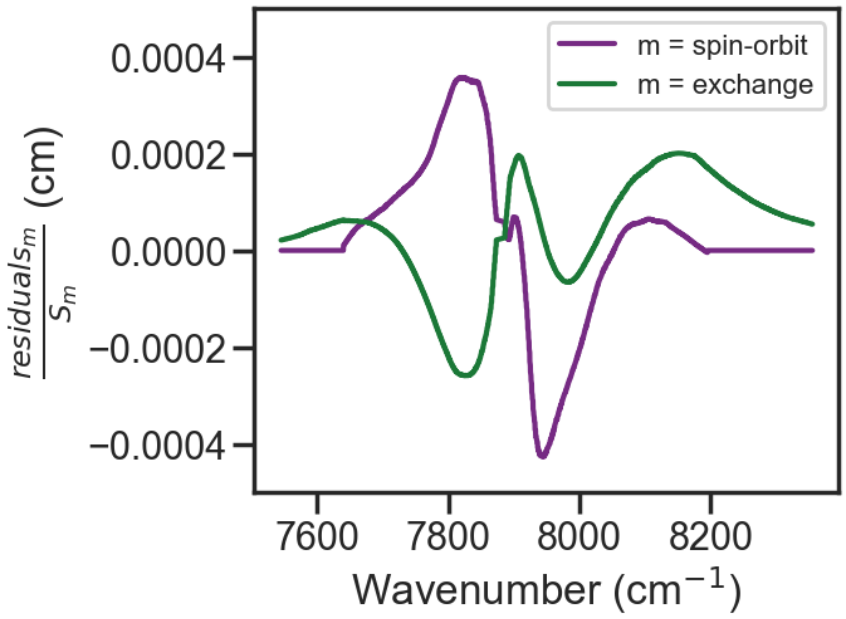

Fig. 6. Spin-orbit and exchange mechanism residuals calculated from the O_2-O_2, and O_2-N_2 residuals, using Eqs. 1 and 2, based on least-squares fits of the respective intensity-scaled, theoretical binary absorption coefficients (with temperature-dependent mechanism intensities) to the combined CRDS data from Fleurbaey [24], Mondelain [13], and Kassi [12].

Improvements to the Calculations of the Theoretical Mechanisms

The demonstrated shortcomings of the theoretical mechanism for the CIA band shapes can be attributed to two main approximations: the first is the model of the electronic transition-dipole surface, and the second is the treatment of the interaction between the molecules. In this work we focused on the 1.27 μm O_2 band, however addressing approximations in the theory would affect the model accuracy for both the 0.76 and 1.27 μm O_2 bands.

For the spin-orbit based mechanism, a simple model of the dipole function was chosen that accounts only for first-order quadrupole induction. The motivation is that spin-orbit coupling mixes the *X* and *b* electronic states, leading to a transition dipole function proportional to both the spin-orbit coupling and the *a* to *b* state transition dipole. This dipole moment is spin-allowed but parity forbidden, and hence gains intensity only by breaking the parity selection rule upon collisions. For the collision-induced *a*-to-*b* transition dipole function, only first-order quadrupole induction was considered because this R^{-4} contribution is usually dominant. However, this quantity can be more accurately determined by including higher-order contributions, as well as modifications of the power-law *R*-dependence at short range. Ultimately, one may even determine the full *a*-to-*b* transition dipole surface from accurate *ab initio* calculations, which would be a considerable effort. Another direction of improvement would be to consider the interaction-induced variation of the spin-orbit coupling, which in principle can also be obtained from *ab initio* calculations [10, 29].

For the exchange-based absorption mechanism, the uncertainty in the transition dipole surface is far greater. As described in detail in Ref. [10, 30], it appears that calculating accurate transition dipole

moments for these nominally spin-forbidden electronic transitions is not possible using current methods for accurate calculations of electronic properties in the ground state. For example, calculations at the CASSCF and MRCI level for various active spaces yield completely different dipole functions. This is highly unusual for "normal" allowed transition dipole functions, and for one-electron properties in general, which are usually qualitatively well-described at the simplest SCF level. Hence, improving upon this exchange-induced transition dipole surface likely requires further method development [10, 29].

Regarding the second approximation involving the interaction between the molecules, the main deficiency is that only isotropic interactions were considered. The effect of anisotropy of the interaction was estimated by computing the integrated intensity by a classical phase-space integral. Including anisotropy increased the intensity by about 50% for the spin-orbit mechanism, and a factor of two to four for the exchange-based mechanism. Hence, there is every reason to believe the effect of interaction anisotropy is substantial, but unfortunately it could not be included in the quantal band shape calculations because this would have prohibitively increased the required computer time. Anisotropic interactions can be included more efficiently in classical simulations [31], but methodology to consider these effects in the modeling of electronic transitions has not yet been developed. Alternatively, one could use classical phase-space integrals to compute higher moments of the spectrum [32] – rather than just the integrated intensity, or zeroth moment – in order to determine crude corrections to the band shape [10].

In addition to the neglect of anisotropic interactions, Karman *et al.* also assumed that the O_2-N_2 and O_2-O_2 interactions are identical. This approximation is possibly less severe than the neglect of anisotropic interactions, but it could be improved upon especially using the new O_2-N_2 potential energy surface in the electronic ground state [33]. Also, *ab initio* calculations of the electronically excited states are possible but might not provide substantial improvements as the differences in potentials between electronic ground and excited state are relatively small.

Conclusions

In this work, we fit parameterized representations of the theoretical CIA published by Karman *et al*. [10] to CRDS measurements of binary absorption coefficients. Measurements for O_2-O_2, O_2-air, and O_2-N_2 [12, 13, 24] performed at NIST and Grenoble were considered. We introduced a model based on the scaled superposition of spin-orbit and exchange mechanisms to adjust the temperature-dependent mechanism intensities to the measured spectra. For all broadener pairs and without adjusting the temperature dependence of the mechanism intensity, the theoretical integrated binary absorption coefficient is within 4.2% of the experiment. When the mechanism intensity is allowed to vary in the fit, experiment and theory differ by 2.7%. Although the agreement between theory and experiment is good, there remain systematic differences in the mechanism-dependent band shapes.

The adjustments to the temperature-dependent intensity mechanisms allow additional flexibility in fitting the theory to measured spectra while maintaining a physical constraint on the overall band shape. Additional degrees of freedom achieved by allowing for the adjustment of the CIA band shapes would provide reduced residuals but would be achieved at the expense of less physically justified band shapes. Advancements in the theory upon which the CIA band shapes are based, namely addressing the approximations made for the electronic transition-dipole surface and the model of the interaction between the molecules would provide more confidence in the theoretical mechanism band shapes and better constraints for data analysis. In this work, we report the spin-orbit and exchange mechanism contributions to the residuals which should be useful for informing future theoretical development. Additional measurements of CIA spanning a broader range of temperatures are also necessary to validate refinements to the theoretical models.

The remaining discrepancy between theory and experiment means that the recommended reference data for the 1.27 μm binary absorption coefficients would be those obtained by combining the data of Fleurbaey [24], Mondelain [13], and Kassi [12] at room temperature, then combining this result with the experimental temperature dependence to achieve the best available accuracy over the reported temperature range. However, the parameterized theoretical model based on the work of Karman *et al*. [10] described in this work has been included in the Multi-spectrum Analysis Tool for Spectroscopy (MATS) [34]. MATS is a multi-spectrum fitting and analysis tool historically used for modeling/simulating line-by-line monomer absorption features. The inclusion of the parameterized theoretical binary absorption coefficient model for O_2-O_2 and O_2-N_2 adds the ability to simultaneously determine monomer absorption and extract CIA from measured spectra by using the theoretical CIA model of Karman *et al*. as a constraint.

Theoretical models of CIA from binary interactions of O_2-O_2 and O_2-N_2 are required to predict the composition, pressure and temperature dependence of absorption cross-sections encountered in the remote sensing of atmospheric O_2. Because of the availability of new variable-temperature CIA data in the 1.27 μm band of O_2 and given that this broadband absorption is much more prominent than in the 0.76 μm band, we chose to apply recent theory for the longer-wavelength CIA by O_2-O_2, O_2-air, and O_2-N_2. We found that the literature data for binary absorption coefficients in the 1.27 μm band are in excellent agreement [10-14, 24], thereby bounding uncertainty of the current calculations and making this band a more appealing target for refinement of the theory. Fig. 7 (bottom) shows much greater experimental discrepancies between CIA cross sections in the 0.76 μm band [10, 11, 18-20, 35, 36] . This follows in part because of the less prominent CIA compared to the monomer absorption (depicted in the middle and top panels of Fig. 7, respectively) and the difficulty in disentangling this broadband effect from that of line-mixing. These differences in measured CIA also far exceed [10-13, 24, 37] those demonstrated here between experiment and theory in the 1.27 μm. Assuming that the theoretical relative uncertainties in band shapes are similar for both spectral regions, then the present theory might provide a realistic constraint on CIA in the 0.76 μm region, although independent experimental confirmation of this assumption would be highly desirable.

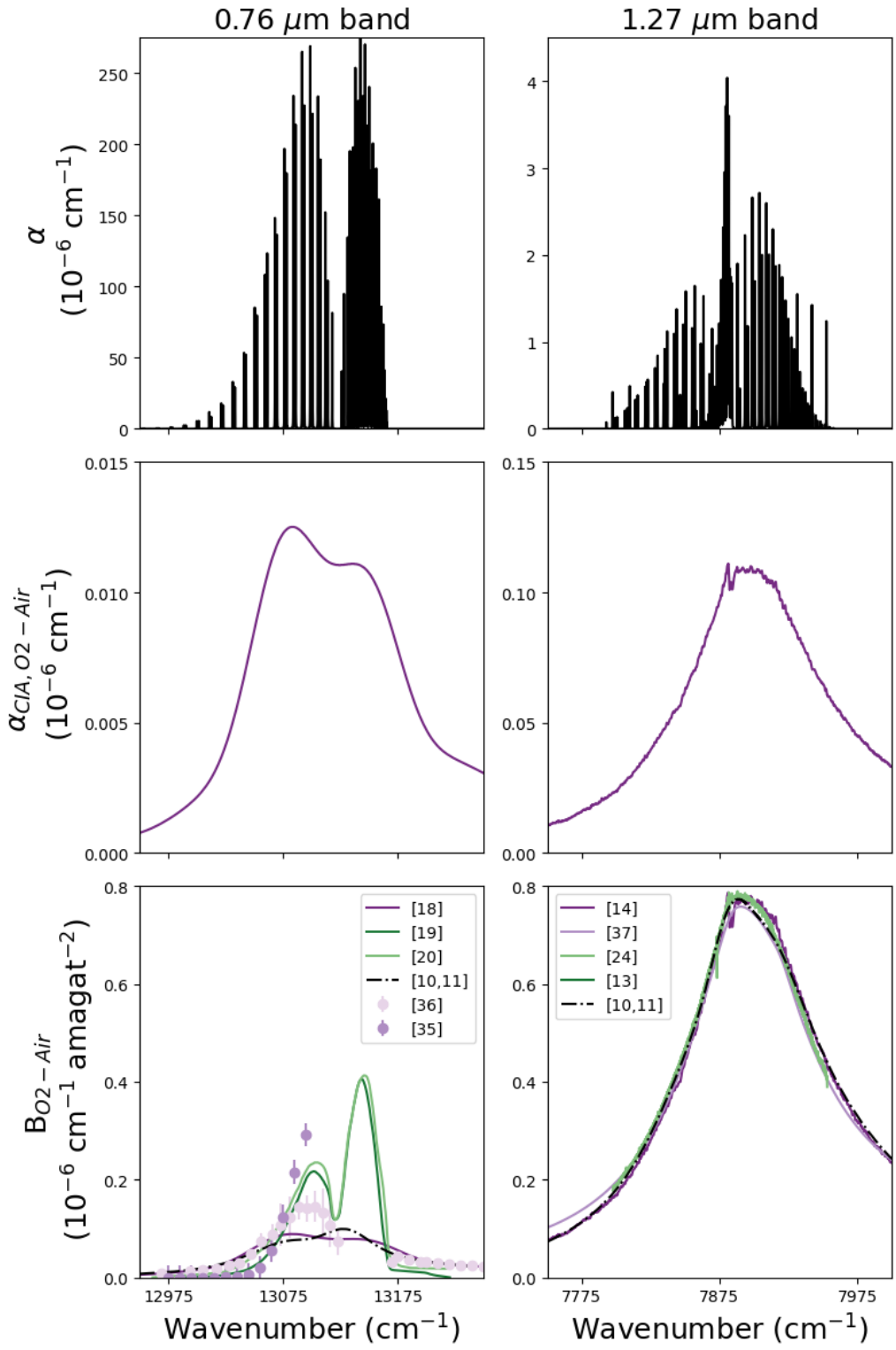

439

440 **Fig. 7.** Top row: Monomer absorption for air simulated using the HITRAN 2020 line list [38] at 296 K and 101.325
441 kPa for the O_2 bands at 0.76 μm (left) and 1.27 μm (right). Middle row: Experimental O_2-air CIA reported in the
442 HITRAN 2019 CIA update [11] originally published by Tran *et al.* for the 0.76 μm [18] and Maté *et al.* for the 1.27
443 μm [14] O_2 bands. Bottom row: Comparison of literature O_2-Air binary absorption coefficients [10, 11, 13, 14, 18-
444 20, 24, 35-37].

References

[1] Crisp D, Atlas RM, Breon FM, Brown LR, Burrows JP, Ciais P, et al. The Orbiting Carbon Observatory (OCO) mission. Advances in Space Research. 2004;34:700-9.

[2] Eldering A, Taylor TE, O'Dell CW, Pavlick R. The OCO-3 mission: measurement objectives and expected performance based on 1 year of simulated data. Atmospheric Measurement Techniques. 2019;12:2341-70.

[3] Butz A, Guerlet S, Hasekamp O, Schepers D, Galli A, Aben I, et al. Toward accurate CO_2 and CH_4 observations from GOSAT. Geophysical Research Letters. 2011;38:n/a-n/a.

[4] Zhu Y, Kaufmann M. Consistent Nighttime Atomic Oxygen Concentrations From O_2 A- band, O(^{1}S) Green- Line, and OH Airglow Measurements as Performed by SCIAMACHY. Geophysical Research Letters. 2019;46:8536-45.

[5] Wunch D, Toon GC, Blavier JF, Washenfelder RA, Notholt J, Connor BJ, et al. The total carbon column observing network. Philos Trans A Math Phys Eng Sci. 2011;369:2087-112.

[6] Sun K, Gordon IE, Sioris CE, Liu X, Chance K, Wofsy SC. Reevaluating the Use of O_2 $a^1\Delta_g$ Band in Spaceborne Remote Sensing of Greenhouse Gases. Geophysical Research Letters. 2018;45:5779-87.

[7] Bertaux J-L, Hauchecorne A, Lefèvre F, Bréon F-M, Blanot L, Jouglet D, et al. The use of the 1.27 μm O_2 absorption band for greenhouse gas monitoring from space and application to MicroCarb. Atmospheric Measurement Techniques. 2020;13:3329-74.

[8] Frey M, Sha MK, Hase F, Kiel M, Blumenstock T, Harig R, et al. Building the COllaborative Carbon Column Observing Network (COCCON): long-term stability and ensemble performance of the EM27/SUN Fourier transform spectrometer. Atmospheric Measurement Techniques. 2019;12:1513-30.

[9] Sodnik Z, Cugny B, Karafolas N, Bernard P, Pascal V, Georges L, et al. The microcarb instrument. International Conference on Space Optics — ICSO 20162017.

[10] Karman T, Koenis MAJ, Banerjee A, Parker DH, Gordon IE, Van Der Avoird A, et al. O_2−O_2 and O_2−N_2 Collision-Induced Absorption Mechanisms Unravelled. Nature Chemistry. 2018;10:549-54.

[11] Karman T, Gordon IE, van der Avoird A, Baranov YI, Boulet C, Drouin BJ, et al. Update of the HITRAN collision-induced absorption section. Icarus. 2019;328:160-75.

[12] Kassi S, Guessoum S, Abanto JCA, Tran H, Campargue A, Mondelain D. Temperature Dependence of the Collision- Induced Absorption Band of O_2 near 1.27 μm. Journal of Geophysical Research: Atmospheres. 2021;126.

[13] Mondelain D, Kassi S, Campargue A. Accurate Laboratory Measurement of the O_2 Collision-Induced Absorption Band near 1.27 μm. Journal of Geophysical Research: Atmospheres. 2019;124:414-23.

[14] Maté B, Lugez C, Fraser GT, Lafferty WJ. Absolute intensities for the O_2 1.27 μm continuum absorption. Journal of Geophysical Research: Atmospheres. 1999;104:30585-90.

[15] Mlawer EJ, Clough SA, Brown PD, Stephen TM, Landry JC, Goldman A, et al. Observed atmospheric collision-induced absorption in near-infrared oxygen bands. Journal of Geophysical Research: Atmospheres. 1998;103:3859-63.

[16] Cho CW, Allin EJ, Welsh HL. Effect of High Pressures on the Infrared and Red Atmospheric Absorption Band Systems of Oxygen. Canadian Journal of Physics. 1963;41:1991-2002.

[17] Blickensderfer RP, Ewing GE. Collision- Induced Absorption Spectrum of Gaseous Oxygen at Low Temperatures and Pressures. I. The $^1\Delta_g \leftarrow {}^3\Sigma_g^-$ System. The Journal of Chemical Physics. 1969;51:873-83.
[18] Tran H, Boulet C, Hartmann JM. Line mixing and collision- induced absorption by oxygen in the A band: Laboratory measurements, model, and tools for atmospheric spectra computations. Journal of Geophysical Research: Atmospheres. 2006;111.
[19] Drouin BJ, Benner DC, Brown LR, Cich MJ, Crawford TJ, Devi VM, et al. Multispectrum analysis of the oxygen A-band. J Quant Spectrosc Radiat Transf. 2017;186:118-38.
[20] Payne VH, Drouin BJ, Oyafuso F, Kuai L, Fisher BM, Sung K, et al. Absorption coefficient (ABSCO) tables for the Orbiting Carbon Observatories: Version 5.1. Journal of Quantitative Spectroscopy and Radiative Transfer. 2020;255.
[21] Tennyson J, Bernath PF, Campargue A, Császár AG, Daumont L, Gamache RR, et al. Recommended isolated-line profile for representing high-resolution spectroscopic transitions (IUPAC Technical Report). Pure and Applied Chemistry. 2014;86:1931-43.
[22] Spiering FR, van der Zande WJ. Collision induced absorption in the $a^1\Delta(v = 2) \leftarrow X^3\Sigma_g^-(v = 0)$ band of molecular oxygen. Phys Chem Chem Phys. 2012;14:9923-8.
[23] Spiering FR, Kiseleva MB, Filippov NN, van Kesteren L, van der Zande WJ. Collision-induced absorption in the O_2 B-band region near 670 nm. Phys Chem Chem Phys. 2011;13:9616-21.
[24] Fleurbaey H, Reed ZD, Adkins EM, Long DA, Hodges JT. High Accuracy Spectroscopic Parameters of the 1.27 μm Band of O_2 Measured with Comb-Referenced, Cavity Ring-Down Spectroscopy. Journal of Quantitative Spectroscopy and Radiative Transfer. 2021;270.
[25] Lafferty WJ, Solodov AM, Lugez C, Fraser GT. Rotational line strength and self-pressure-broadening coefficients for the 1.27-μm, a $^1\Delta_g$-$X^3\Sigma_g^-$, v = 0-0 band of O_2. Appl Opt. 1998;37:2264-70.
[26] Gordon IE, Rothman LS, Hill C, Kochanov RV, Tan Y, Bernath PF, et al. The HITRAN2016 molecular spectroscopic database. 2017;203:3-69.
[27] Tran DD, Delahaye T, Armante R, Hartmann JM, Mondelain D, Campargue A, et al. Validation of spectroscopic data in the 1.27 μm spectral region by comparisons with ground-based atmospheric measurements. Journal of Quantitative Spectroscopy and Radiative Transfer. 2021;261.
[28] Fleurbaey H, Yi H, Adkins EM, Fleisher AJ, Hodges JT. Cavity ring-down spectroscopy of CO_2 near λ = 2.06 μm: Accurate transition intensities for the Orbiting Carbon Observatory-2 (OCO-2) "strong band". Journal of Quantitative Spectroscopy and Radiative Transfer. 2020;252:107104.
[29] Karman T, Van Der Avoird A, Groenenboom GC. Line-shape theory of the $X^3\Sigma_g^- \rightarrow a^1\Delta_g$, $b^1\Sigma_g^+$ transitions in O_2–O_2 collision-induced absorption. The Journal of Chemical Physics. 2017;147:084307.
[30] Karman T, van der Avoird A, Groenenboom GC. Potential energy and dipole moment surfaces of the triplet states of the $O_2(X^3\Sigma_g^-) \rightarrow O_2(X^3\Sigma_g^-, a^1\Delta_g, b^1\Sigma_g^+)$ complex. J Chem Phys. 2017;147:084306.
[31] Hartmann J-M, Boulet C, Jacquemart D. Molecular dynamics simulations for CO_2 spectra. II. The far infrared collision-induced absorption band. The Journal of chemical physics. 2011;134:094316.
[32] Frommhold L. Collision-induced Absorption in Gases1994.

[33] Gancewski M, Jozwiak H, Quintas-Sanchez E, Dawes R, Thibault F, Wcislo P. Fully quantum calculations of O_2-N_2 scattering using a new potential energy surface: Collisional perturbations of the oxygen 118 GHz fine structure line. J Chem Phys. 2021;155:124307.
[34] Adkins EM. Multi-spectrum Analysis Tool for Spectroscopy (MATS). 2020. https://doi.org/10.18434/M32200.
[35] Long DA, Robichaud DJ, Hodges JT. Frequency-stabilized cavity ring-down spectroscopy measurements of line mixing and collision-induced absorption in the O2 A-band. J Chem Phys. 2012;137:014307.
[36] Spiering FR, Kiseleva MB, Filippov NN, Naus H, van Lieshout B, Weijenborg C, et al. Line mixing and collision induced absorption in the oxygen A-band using cavity ring-down spectroscopy. J Chem Phys. 2010;133:114305.
[37] G.C.Toon BS, A.Kleinboehl. DERIVATION OF PSEUDO-LINES FROM LABORATORY CROSS-SECTIONS. Jet Propulsion Laboratory.
[38] Gordon IE, Rothman LS, Hargreaves RJ, Hashemi R, Karlovets EV, Skinner FM, et al. The HITRAN2020 molecular spectroscopic database. Journal of Quantitative Spectroscopy and Radiative Transfer. 2021.